Infrared Physics & Technology 77 (2016) 226–229

Contents lists available at ScienceDirect

Infrared Physics & Technology

journal homepage: www.elsevier.com/locate/infrared

Far-infrared spectra of dysprosium doped yttrium aluminum garnet nanopowder

J. Trajić [a,*], M.S. Rabasović [a], S. Savić-Šević [a], D. Šević [a], B. Babić [b], M. Romčević [a], J.L. Ristić-Djurović [a], N. Paunović [a], J. Križan [c], N. Romčević [a]

[a] Institute of Physics, University of Belgrade, Pregrevica 118, 11080 Belgrade, Serbia
[b] Vinca Institute of Nuclear Sciences, University of Belgrade, 11001 Belgrade, Serbia
[c] AMI, d.o.o., Ptuj, Slovenia

HIGHLIGHTS

- YAG:Dy nanopowder was produced by Solution Combustion Synthesis (SCS) method.
- Powders are composed by well-defined and separated nanoparticles.
- Some particles are agglomerated but there are also separated particles.
- The dielectric function was modeled by the Maxwell–Garnet formula.
- Optical phonon confinement is registered.

GRAPHICAL ABSTRACT

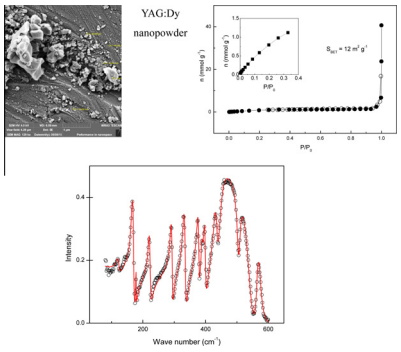

ARTICLE INFO

Article history:
Received 20 April 2016
Revised 8 June 2016
Accepted 9 June 2016
Available online 9 June 2016

Keywords:
$Y_3Al_5O_{12}$
Dy^{3+}
Nanopowders
Light absorption and reflection

ABSTRACT

The solution combustion synthesis was used to prepare nanopowders of yttrium aluminum garnet (YAG) and YAG doped with dysprosium ions, Dy^{3+}, (YAG:Dy). The morphology, specific surface area, texture, and optical properties of the prepared materials were studied by the means of scanning electron microscopy (SEM), nitrogen adsorption method, and far-infrared spectroscopy at room temperature in the spectral region between 80 and 600 cm^{-1}. It was established that all the examined samples were microporous. The Maxwell–Garnet formula was used to model dielectric function of YAG and YAG:Dy nanopowders as mixtures of homogenous spherical inclusions in air.

1. Introduction

Importance of yttrium aluminum garnet, $Y_3Al_5O_{12}$, commonly abbreviated as YAG, arises from its high chemical stability as well as excellent optical and high-temperature mechanical properties [1]. It is a ceramic material with a cubic garnet crystallographic structure whose thermal expansion is isotropic, whereas its optical properties are homogeneous, without birefringence effects [2,3]. Over the last five decades the structural properties of YAG were the subject of numerous studies, which proved its technological relevance and led to its use in a broad range of applications. For example, YAG has found its role as a host material in solid-state lasers of different kinds, luminescence materials, and scintillators [4–6].

Two prospective applications particularly draw attention toward trivalent dysprosium-activated optical materials. Namely,

* Corresponding author.
E-mail address: jelena@ipb.ac.rs (J. Trajić).

http://dx.doi.org/10.1016/j.infrared.2016.06.003
1350-4495/

if the phonon energy of host matrix is low, these materials could be an alternative to praseodymium-doped optical amplifiers used in the second telecommunication window [7]. The second promising area of application, the solid-state lasers operating in the visible part of the spectrum [8], is based on the blue and yellow emissions originating from $^4F_{9/2}$ level of Dy^{3+}. These emissions are much more probable than the non-radiative relaxation to the next lower energy level, $^6F_{3/2}$, that corresponds to large energy gap of approximately 7500 cm^{-1}. Consequently, relatively high phonon energy of yttrium aluminum garnet presents YAG crystal as a prospective host material for dysprosium ions [9].

We used solution combustion synthesis (SCS) method to prepare nanopowder samples of YAG and YAG doped with 2 mol% Dy. Optical properties of the samples were analyzed by far-infrared spectroscopy (FIR), whereas nitrogen adsorption method was employed to examine specific surface area and texture. The dielectric function of the nanopowders was modeled using the Maxwell–Garnet formula.

2. Samples preparation and characterization

The SCS method used to prepare the YAG and YAG:Dy nanopowder samples was performed in several steps. Yttrium oxide (Y_2O_3) and aluminum oxide (Al_2O_3) of 99.99 % purity was purchased from the NOAH Technologies. The oxides were dissolved in HNO_3 followed by the addition of carbohydrazide to the solution of aluminum nitrate and yttrium nitrate:

$$3Y(NO_3)_3 + 5Al(NO_3)_3 + 15CH_6N_4O \rightarrow YAG + 42N_2 + 15CO_2 + 45H_2O.$$

Good reactivity of the raw materials provided absence of the intermediate phases, e.g., YAM ($Y_4Al_2O_9$) or YAP ($YAlO_3$), in the obtained YAG powder. The YAG:Dy samples were produced by doping YAG host with Dy^{3+} ions using the concentration of 2 mol %. Further, YAG:Dy nanopowder was annealed in the air atmosphere at 1300 °C with the aim to obtain full crystallinity [10].

The morphology of the prepared YAG and YAG:Dy nanopowders was examined using a high resolution scanning electron microscope (SEM) equipped with the high brightness Schottky Field Emission gun (FEGSEM, TESCAN) operating at 4 kV. In order to provide conductivity of the samples needed for SEM analysis, the samples were coated with gold/palladium. The SEM images of our YAG and YAG:Dy samples are given in Fig. 1. The powders are composed of well-defined and separated nanoparticles, clusters, and agglomerated particles. The size of individual spherical particles is in the range of about 30–50 nm. The spherical shape of particles is of great importance because it provides lower light scattering and brighter luminescence performance [11].

3. Results and discussion

3.1. Adsorption isotherms – BET experiments

The analyzer Surfer (Thermo Fisher Scientific, USA) was used to examine YAG and YAG:Dy nanopowders.

The dependences of the adsorbed amount of N_2 on the relative pressure, P/P_0, at the temperature of −196 °C, i.e., the nitrogen adsorption isotherms, for the YAG and YAG:Dy samples are given in Fig. 2. The adsorptions at low relative pressures, given in the graph inserts, indicate that there are micropores on the particle surfaces. According to the IUPAC classification pores are classified as macropores (pore width above 50 nm), mesopores (pore width 2–50 nm) and micropores (pore width below 2 nm) [12]. At the same time, non-limiting adsorption at high P/P_0, was found to correspond to non-rigid aggregates of particles giving rise to slit-shaped pores [13]. Note that these conclusions are in agreement with the SEM images given in Fig. 1, which show that our samples contain agglomerated as well as separated particles. The separated particles are found to be spherical with the diameter of approximately 40 nm. The specific surface areas calculated by the BET equation, S_{BET}, are found to be 5 $m^2\,g^{-1}$ and 12 $m^2\,g^{-1}$ for the YAG and YAG:Dy samples, respectively. Since the radius of Dy^{3+} ion of 0.1167 nm is larger than the radius of Y^{3+} ion, which is 0.1159 nm, it comes as no surprise that the presence of Dy led to increase of the overall specific surface of particles. Also, dopants introduce defects into the structure of the material which results in different charge on the particle surface when doped and undoped are compared. This charge on the particle surface leads to differences in packaging particles and their greater or lesser agglomeration, which on the other hand have significant role on the porosity and specific surface area. Incorporated dopants have a tendency to concentrate at the surface of nanomaterials. All these have significant role on the increasing of the specific surface area.

3.2. Far-infrared spectroscopy

The far-infrared measurements were carried out with the BOMEM DA – 8 FIR spectrometer. The wave number range between 80 and 600 cm^{-1} was covered with the DTGS pyroelectric detector.

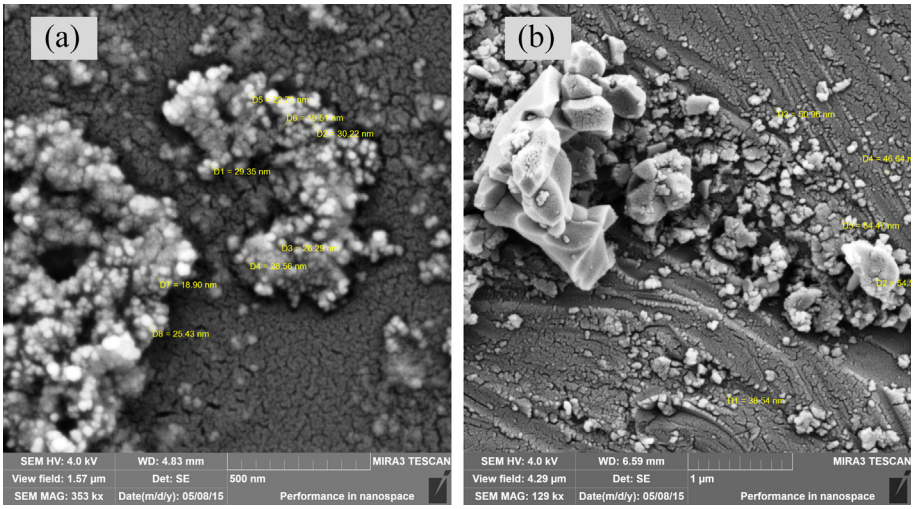

Fig. 1. SEM micrographs. The micrographs of YAG and YAG:Dy nanopowders are given in part (a) and (b), respectively.

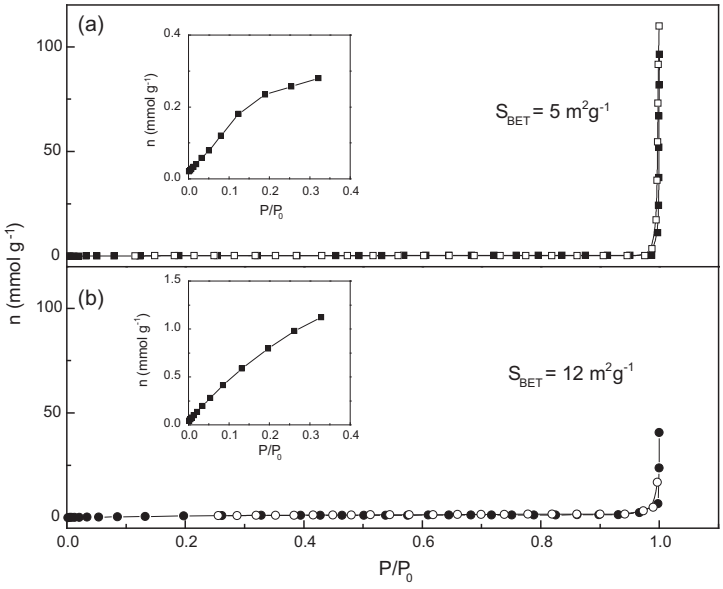

Fig. 2. Nitrogen adsorption isotherms. The amount of adsorbed N_2 given as a function of the relative pressure is shown in graphs (a) and (b) for YAG and YAG:Dy nanopowders, respectively. Solid symbols correspond to adsorption, whereas open symbols represent desorption. The shapes of the curves around zero are enlarged in the inserts.

If the visible light wavelength, λ, is much larger than the characteristic size of semiconducting nanoparticles, d, i.e., if $\lambda \gg d$, the heterogeneous composite of nanoparticles with the dielectric function ε_2 distributed in a medium with the dielectric constant ε_1 can be treated as a homogeneous medium and effective medium theory is applicable. The effective dielectric permittivity of such a mixture can be modeled by a number of mixing models [14]. We chose the Maxwell–Garnet model since our samples are well defined and separated nanosized spherical grains. Consequently, the predicted effective permittivity of the mixture becomes [15]:

$$\varepsilon_{eff} = \varepsilon_1 + 3f\varepsilon_1 \frac{\varepsilon_2 - \varepsilon_1}{\varepsilon_2 + 2\varepsilon_1 - f(\varepsilon_1 - \varepsilon_2)}, \quad (1)$$

where spheres of permittivity ε_2 were taken to occupy a volume fraction f as well as to be randomly located in a homogeneous environment characterized with ε_1. In the considered nanopowders, nanoparticles are situated in air, therefore $\varepsilon_1 = 1$. To determine the dielectric function of the nanoparticles, i.e., ε_2, we used the plasmon–phonon interaction model [16]:

$$\varepsilon_2(\omega) = \varepsilon_\infty \left(\prod_{k=1}^{n} \frac{\omega_{LOk}^2 - \omega^2 + \imath\gamma_{LOk}\omega}{\omega_{TOk}^2 - \omega^2 + \imath\gamma_{TOk}\omega} - \frac{\omega_P^2}{\omega(\omega - \imath\tau^{-1})} \right) \quad (2)$$

where ε_∞ is the bound charge contribution and it is assumed to be a constant, ω_{TOk} and ω_{LOk} are the transverse and longitudinal frequencies, $\gamma_{TOk,}$ and γ_{LOk} are their dampings, ω_P is the plasma frequency and τ is the free carrier relaxation time. The first term in Eq. (2) is the lattice contribution, whereas the second term corresponds to the Drude expression for the free carrier contribution to the dielectric constant.

The measured and calculated far-infrared spectra of YAG and YAG:Dy nanopowders, in the spectral range between 80 and 600 cm^{-1}, at room temperature are shown in Fig. 3. The experimental data are depicted by circles, whereas the solid lines are used to draw the calculated spectra obtained by the fitting procedure based and the model defined by Eqs. (1) and (2). The best fit parameters corresponding to YAG and YAG:Dy nanopowders are given in Table 1. The values corresponding to the YAG single crystal are taken from [17].

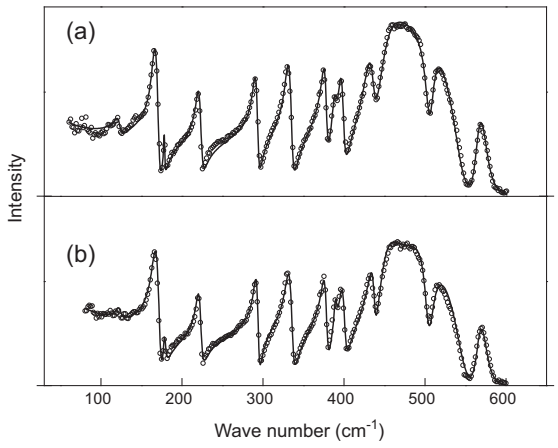

Fig. 3. Far-infrared reflection spectra of YAG nanopowder (a) and YAG:Dy nanopowder (b) at room temperature. The experimental data are represented by circles. The solid lines are the calculated spectra obtained with the parameter values given in Table 1 and the fitting procedure based on the model given by Eqs. (1) and (2).

YAG crystallizes in the cubic structure, it has the symmetry of O_h^{10}–$Ia3d$ space group, and eight molecules of $Y_3Al_5O_{12}$ per primitive unit cell. Out of the ninety-eight theoretically predicted Brillouin zone center modes that correspond to the O_h structure in the YAG group, $3A_{1g} + 5A_{2g} + 8E_g + 14T_{1g} + 14T_{2g} + 5A_{1u} + 5A_{2u} + 10E_u + 18T_{1u} + 16T_{2u}$, only the eighteen T_{1u} modes are IR-active [19]. Further, out of these eighteen theoretically predicted IR-active modes, fourteen are visible in the experimental and modeled far-infrared reflectivity spectra of the YAG and YAG:Dy nanopowders, and in the data corresponding to the YAG single crystal retrieved from literature, see Fig. 3 and Table 1. The bands at around 430, 453, 477, 510 and 566 cm^{-1} represent the characteristic metal–oxygen vibrations, which are in our example Y–O and Al–O. Our data are in agreement with the previous reports regarding single crystals [18,19] as well as with the results on nanocrystals of YAG [20,21]. The peaks located in the vicinity of 477, 510 and 566 cm^{-1} are the asymmetric stretching vibrations, whereas the peak at approximately 453 cm^{-1} is the symmetric vibration

Table 1
Best fit parameters of far-infrared spectra of YAG single crystal, YAG nanopowder and YAG:Dy nanopowder.

	YAG single crystal	YAG nanopowder	YAG:Dy nanopowder	Vibrations
ω_{TO} (cm^{-1})	122	122	122	T (+T_d) translations of tetrahedral and dodecahedral cation
	165	165	163	T_d translations of dodecahedral cation
	180	178	178	T_d (+T) translations of tetrahedral and dodecahedral cation
	221	220	219	T_d translations of dodecahedral cation (translations of cations in YO_3 and AlO_4)
	291	290	289.5	T_0
	327	330	328	T translations of tetrahedral cation
	375	375	373	R libration of tetrahedral cation
	390	388.5	389	T_0 translations of octahedral cation
	396	399.5	396	R libration of tetrahedral cation
	432	431	431	T_0 translations of octahedral (translations + libration) cations in AlO_6 and AlO_4
	453	447	444	ν_2 symmetric
	477	465	465	ν_4 symmetric
	510	508	507	ν_4
	566	563	564	ν_4 (symmetric and asymmetric stretching of Al–O in octahedrons)
ω_p (cm^{-1})	220	190	220	–
τ (cm^{-1})	0.001	0.002	0.035	–
f	1	0.96	0.80	–

of Al–O bond in the octahedral arrangement of garnet structure. The four lowest energy peaks correspond to the translation and vibration of cations in different coordination – tetrahedral, octahedral and dodecahedral [22]. The peaks around 165, 220, 375 and 396 cm^{-1} have been attributed to the translator motion of Y^{3+} ions within the distorted cube that has eight oxygen ions at its vertices, as well as to the heavy mixing of the translational, rotational, and ν_3 mode of the (AlO_4) unit.

Differences in the structure of YAG single crystal and YAG nanopowder cause changes in the phonon frequencies. Namely, decrease in the crystallite size causes optical phonon confinement. The influence of doping of YAG by Dy^{3+} on the spectral properties and lattice vibrations is not significant. Compared to the spectra of YAG single crystal and YAG nanopowder, there are no new phonon modes corresponding to the YAG:Dy nanopowder; however, further decrease of phonon frequencies is registered. Since Dy^{3+} ions are by 0.69%, larger than Y^{3+} ions, substitution of Y^{3+} with Dy^{3+} leads to further distortion of the cubic cell, and consequently to the shift of characteristics frequencies toward lower frequencies, as can be seen in Fig. 3 and Table 1.

The values of filling factors were determined from the analysis of reflection spectra. The main volume fraction, f, obtained as the best fit parameter estimation, is listed in Table 1. These results are consistent with the results obtained by the BET experiment described in Section 3.1. Namely, high values of the filling factor are associated with the existence of micropores.

4. Conclusions

Due to their prospective application in optical amplifiers for the second telecommunication window and solid-state lasers that operate in the visible part of the spectrum, properties of the YAG:Dy nanopowder were investigated and compared to those corresponding to the YAG nanopowder and YAG single crystal. The nanopowders were synthetized by the solution combustion synthesis technique and the samples were analyzed by the scanning electron microscopy, nitrogen adsorption method as well as by the far-infrared spectroscopy. The measured far-infrared spectra were in complete agreement with the modeled spectra obtained with the Maxwell–Garnet formula, plasmon–phonon interaction model, and fitting procedure. It was determined that the Dy doped as well as non-doped YAG nanopowders are microporous. Spherical, well-defined and separated nanoparticles as well as agglomerated particles were detected. The far-infrared measurements revealed that the YAG nanopowder has lower phonon frequencies than the YAG single crystal as well as that doping of YAG by Dy^{3+} does not have significant influence on the spectral properties and lattice vibrations. However, the doping caused further decrease of phonon frequencies, with respect to the frequencies that correspond to the YAG single crystal and YAG nanopowder.

Acknowledgment

This work was supported by the Serbian Ministry of Education, Science and Technological Development under Project III45003.

References

[1] Ji-Guang Li, Takayasu Ikegami, Jong-Heun Lee, Toshiyuki Mori, J. Am. Ceram. Soc. 83 (4) (2000) 961–963.
[2] L. Wen, X. Sun, Z. Xiu, S. Chen, Chi-Tay Tsai, J. Eur. Ceram. Soc. 24 (2004) 2681–2688.
[3] J.W.G.A. Vrolijk, J.W.M.M. Willems, R. Metselaar, J. Eur. Ceram. Soc. 6 (1990) 47–51.
[4] Y. Fujimoto, T. Yanagida, H. Yagi, T. Yanagidani, V. Chani, Opt. Mater. 36 (2014) 1926–1929.
[5] C.R. Varney, D.T. Mackay, S.M. Reda, F.A. Selim, J. Phys. D Appl. Phys. 45 (2012) 015103–015106.
[6] A. Senyshyn, L. Vasylechko, Acta Phys. Pol., A 124 (2013) 329–335.
[7] B. Cole, L.B. Shaw, P.C. Pureza, R. Mossadegh, J.S. Sanghera, I.D. Aggarwal, J. Non-Cryst, Solids 256–257 (1999) 253–259.
[8] A. Kaminskii, U. Hommerich, D. Temple, J.T. Seo, K.-I. Ueda, S. Bagayev, A. Pavlyulk, Jpn. J. Appl. Phys., Part 2: Lett. 39 (3A/B) (2000). L208-11.
[9] M. Klimczak, M. Malinowski, J. Sarnecki, R. Piramidowic, J. Lumin. 129 (2009) 1869–1873.
[10] M.S. Rabasovic, D. Sevic, J. Krizan, M.D. Rabasovic, S. Savic-Sevic, M. Mitric, M. Petrovic, M. Gilic, N. Romcevic, Opt. Mater. 50 (2015) 250–255.
[11] Joo-Yun Chong, Yuelan Zhang, Brent K. Wagner, Zhitao Kang, J. Alloys Compd. 581 (2013) 484–487.
[12] K.S.W. Sing, D.H. Everett, R.A.W. Haul, L. Moscou, R.A. Pierotti, J. Rouquerol, et al., Pure Appl. Chem. 57 (4) (1985) 603–619.
[13] S. Lowell, J.E. Shields, M.A. Thomas, M. Thommes, Charactrization of Porous Solids and Powders: Surface Area, Pore Size and Density, Kluwer Academic Publishers, Dordrecht Netherlands, 2004. 44.
[14] K. Karkkainen, A. Saviola, K. Nikoskinen, IEEE Trans. Geosci. Remote Sensors 39 (5) (2001) 1013–1018.
[15] J.C.M. Garnett, Trans. R. Soc. Vol. CCIII (1904) 385–420.
[16] I.J. Uhanov, Opt. svojstva poluprovodnikov, Nauka, Moskva (1977).
[17] S. Kostić, Z.Ž. Lazarević, V. Radojević, A. Milutinović, M. Romčević, N.Ž. Romčević, A. Valčić, Mater. Res. Bull. 63 (2015) 80–87.
[18] J.P. Hurrel, P.S. Porto, I.F. Chang, S.S. Mitra, R.P. Bauman, Phys. Rev. 173 (1968) 851–856.
[19] G.A. Slack, D.W. Oliver, R.M. Chrenko, S. Roberts, Phys. Rev. 177 (1969) 1308–1314.
[20] Z.H. Chen, Y. Yang, Z.G. Hu, J.-T. Li, S.L. He, J. Alloys Compd. 433 (2007) 328–331.
[21] E. De la Rosa, L.A. Díaz-Torres, P. Salas, A. Arredondo, J.A. Montoya, C. Angeles, R.A. Rodríguez, Opt. Mater. 27 (2005) 1793–1799.
[22] A.M. Hofmeister, K.R. Campbell, J. Appl. Phys. 72 (1992) 638–646.